Vol 16 No 11, November 2007
1009-1963/2007/16(11)/3285-05

Chinese Physics

© 2007 Chin. Phys. Soc.
and IOP Publishing Ltd

Analysis of second-harmonic generation microscopy under refractive index mismatch

Wang Xiang-Hui(王湘晖)[a)b)†], Lin Lie(林 列)[a)b)], and Zhang Yang(张 杨)[a)b)]

[a)] *The Key Laboratory of Opto-electronic Information Science and Technology, the Ministry of Education, Tianjin* 300071, *China*

[b)] *Institute of Modern Optics, Nankai University, Tianjin* 300071, *China*

(Received 7 October 2006; revised manuscript received 17 April 2007)

On the basis of the vector diffraction theory and Green's function method, this paper investigates the effects of refractive index mismatch on second-harmonic generation (SHG) microscopy. The polarization distribution and SHG intensity are calculated as functions of the sample radius and probe depth. The numerical results show that refractive index mismatch can result in peak intensity degradation, increase secondary lobes and extension of second-harmonic polarization distribution. Because of the attenuation of polarization intensity, the detected SHG intensity significantly decreases with increasing probe depth, which can limit the imaging depth of SHG microscopy inside thick samples. Forward SHG intensity decays slowly than backward SHG, due to the combination of extension second-harmonic polarization distribution and strong dependency of forward SHG on sample radius.

Keywords: microscopy, second-harmonic generation, polarization, refractive index mismatch
PACC: 0760P, 4265J

1. Introduction

In recent years, there has been increasing interest in the use of nonlinear optical process for microscopy[1−5] among which second-harmonic generation (SHG) is one of them. Due to its nonlinear nature, the SHG intensity depends on the square of the excitation light intensity. Similar to two-photon induced fluorescence processes, this nonlinear dependency results in signal generation only from the focal volume and allows three-dimensional imaging of thick samples with submicron spatial resolution. The near-infrared light source used for SHG microscopy also provides deep penetration into biological tissues without complex physical sectioning and fixing processes. Moreover, SHG microscopy can readily provide direct information about the sample without photobleaching and additional staining with fluorochrome, which is superior to two-photon fluorescence microscopy. As an important imaging modality in nonlinear optical microscopy, SHG microscopy has been applied to study collagen,[1] live cell,[2] muscle[3] and in-vivo developmental biology.[4]

On the basis of the paraxial approximation or the vector approach, many papers have dealt with the theory of SHG by focused laser beams.[6−8] However, most of them did not consider the effects of refractive index mismatch on SHG microscopy. In reality, the refractive index of immersion oil often mismatches with that of biological samples, which is significant for lens with high numerical aperture (NA) and can cause changes of the electric field distribution in the focal region featuring a degraded and displaced peak amplitude, increase secondary lobes and extent full width of half-maximum (FWHM).[9,10] In this paper, on the basis of the vector diffraction theory and Green's function method, we investigate the effects of refractive index mismatch on SHG microscopy by analysing the changes of the second-harmonic polarization distribution and SHG signal with increasing probe depth. The numerical results show that the imaging depth of SHG microscopy inside thick samples can be limited by SHG signal degradation with increasing probe depth, due to aberration introduced by refractive index mismatch.

2. Theory

Let us consider a high NA lens free of aberrations that is illuminated by a laser beam which propagates along the z axis and is linearly polarized in the x di-

†E-mail: wangxianghui@mail.nankai.edu.cn

rection.

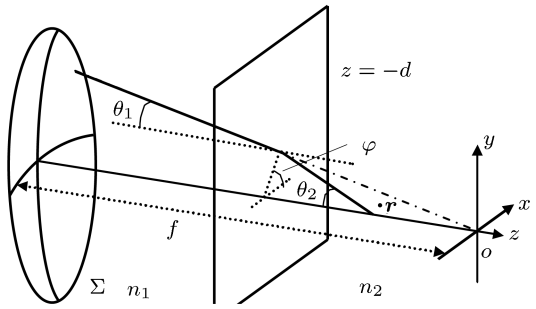


Fig.1. Geometry when focusing with refractive index mismatch.

As shown in Fig.1, when the beam is focused through a planar interface separating two media with refractive indices n_1 and n_2, the electric field of arbitrary point $\boldsymbol{r}$ in the focal region can be described as[9,10]

$$\begin{aligned} E_x(\boldsymbol{r}) &= -\mathrm{i}\Big(\frac{k_2}{k_1}\Big)^2 A[I_0 + I_2\cos(2\varphi)],\\ E_y(\boldsymbol{r}) &= -\mathrm{i}\Big(\frac{k_2}{k_1}\Big)^2 A I_2 \sin(2\varphi),\\ E_z(\boldsymbol{r}) &= -2\Big(\frac{k_2}{k_1}\Big)^2 A I_1 \cos(\varphi), \end{aligned} \tag{1}$$

where k_1 and k_2 denote the wave number of the incident light in the first and second medium, respectively. ϕ is the azimuth angle of the point $\boldsymbol{r}$ in the focal region. A is proportional to the field amplitude on the exit pupil. The integrals I_n are defined by

$$\begin{aligned} I_0 &= \int_0^{\alpha} (\cos\theta_1)^{1/2}(\sin\theta_1)\exp[\mathrm{i}k_0\psi(\theta_1,\theta_2,-d)](\tau_\mathrm{s}+\tau_\mathrm{p}\cos\theta_2)J_0\Big(\frac{v\sin\theta_1}{\sin\alpha}\Big)\exp\Big(\frac{\mathrm{i}u\cos\theta_2}{\sin^2\alpha}\Big)\mathrm{d}\theta_1,\\ I_1 &= \int_0^{\alpha} (\cos\theta_1)^{1/2}(\sin\theta_1)\exp[\mathrm{i}k_0\psi(\theta_1,\theta_2,-d)]\tau_\mathrm{p}(\sin\theta_2)J_1\Big(\frac{v\sin\theta_1}{\sin\alpha}\Big)\exp\Big(\frac{\mathrm{i}u\cos\theta_2}{\sin^2\alpha}\Big)\mathrm{d}\theta_1,\\ I_2 &= \int_0^{\alpha} (\cos\theta_1)^{1/2}(\sin\theta_1)\exp[\mathrm{i}k_0\psi(\theta_1,\theta_2,-d)](\tau_\mathrm{s}-\tau_\mathrm{p}\cos\theta_2)J_2\Big(\frac{v\sin\theta_1}{\sin\alpha}\Big)\exp\Big(\frac{\mathrm{i}u\cos\theta_2}{\sin^2\alpha}\Big)\mathrm{d}\theta_1, \end{aligned} \tag{2}$$

where J_n is the Bessel function of the first kind order n, and τ_s, τ_p are the Fresnel transmission coefficients.[11] θ_1 and θ_2 represent the polar angle in the first and second medium, respectively. α denotes the aperture half-angle of the objective lens. The optical co-ordinates u and v are defined by

$$u = k_2 z\sin^2(\alpha), \quad v = k_1\sqrt{x^2+y^2}\,\sin(\alpha). \tag{3}$$

The aberration function ψ is

$$\psi(\theta_1,\theta_2,-d) = -d(n_1\cos\theta_1 - n_2\cos\theta_2), \tag{4}$$

where d represents the distance between the Gaussian focus and the interface plane, also the probe depth.

In SHG microscopy, the focused laser field interacts with a sample and generates a second-harmonic polarization field. The nonlinear optical property of the sample is usually described by a nonlinear susceptibility tensor. Here, we assume that a hypothetical collagen fibril, which is a very good second harmonic generator, is placed in the focal region. The tensor of the hypothetical collagen fibril is described as a C_6 tensor. When the axis of symmetry is parallel to the z axis and the incident light is polarized in the x direction, the induced second-harmonic polarization is expressed as[3,7]

$$\begin{bmatrix} P_x^{2\omega}(\boldsymbol{r})\\ P_y^{2\omega}(\boldsymbol{r})\\ P_z^{2\omega}(\boldsymbol{r}) \end{bmatrix} = \begin{bmatrix} 0 & 0 & 0 & 0 & d_{xxz} & 0\\ 0 & 0 & 0 & d_{yyz} & 0 & 0\\ d_{zxx} & d_{zyy} & d_{zzz} & 0 & 0 & 0 \end{bmatrix} \begin{bmatrix} E_xE_x\\ E_yE_y\\ E_zE_z\\ 2E_yE_z\\ 2E_xE_z\\ 2E_xE_y \end{bmatrix}, \tag{5}$$

where d_{ijk} take the values $d_{xxz} = d_{yyz} = 1.15$, $d_{zxx} = d_{zyy} = 1$ and $d_{zzz} = 0.09$.

The SHG signal field is calculated as a coherent superposition of the radiation fields from the second-harmonic polarization generated inside the sample and satisfies the inhomogeneous wave equation.[12] This wave equation can be resolved by use of Green's function approach.[13,14] For far-field radiation ($R \gg r$), the radiation pattern of SHG can be presented in spherical coordinates:[7,15]

$$\boldsymbol{E}^{2\omega}(\boldsymbol{R}) = \frac{\exp(\mathrm{i}2k_2R)}{R}\iiint_V \mathrm{d}V\exp\Big(\frac{-\mathrm{i}2k_2\boldsymbol{R}\cdot\boldsymbol{r}}{R}\Big)\begin{bmatrix} 0 & 0 & 0 \\ \cos\Theta\cos\Phi & \cos\Theta\sin\Phi & -\sin\Theta \\ -\sin\Phi & \cos\Phi & 0 \end{bmatrix}\begin{bmatrix} P_x^{2\omega}(\boldsymbol{r}) \\ P_y^{2\omega}(\boldsymbol{r}) \\ P_z^{2\omega}(\boldsymbol{r}) \end{bmatrix}. \quad (6)$$

Here, Θ and Φ are the polar and azimuthal angles of the observation point $\boldsymbol{R}$, respectively.

When the signal is collected by a lens, the SHG intensity can be calculated by integrating the second-harmonic signal over a spherical surface:

$$I^{2\omega} = \int_0^{\alpha}\mathrm{d}\,\Theta\int_0^{2\pi}\mathrm{d}\,\Phi|\boldsymbol{E}^{2\omega}(\boldsymbol{R})|^2R^2\sin\Theta. \quad (7)$$

3. Results and discussion

In the following calculations the focusing and collecting objectives are assumed to have the same NA, 1.4. The refractive index of immersion oil ($n_1 = 1.5$) mismatches with that of the sample ($n_2 = 1.4$). The excitation wavelength is 1200nm and the amplitude of incident light is considered to be uniform in the transverse plane.

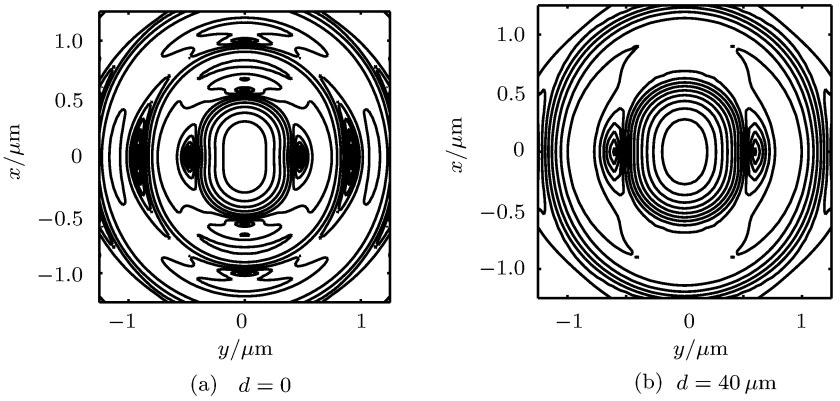


Fig.2. The contours of second-harmonic polarization distributions in xy plane.

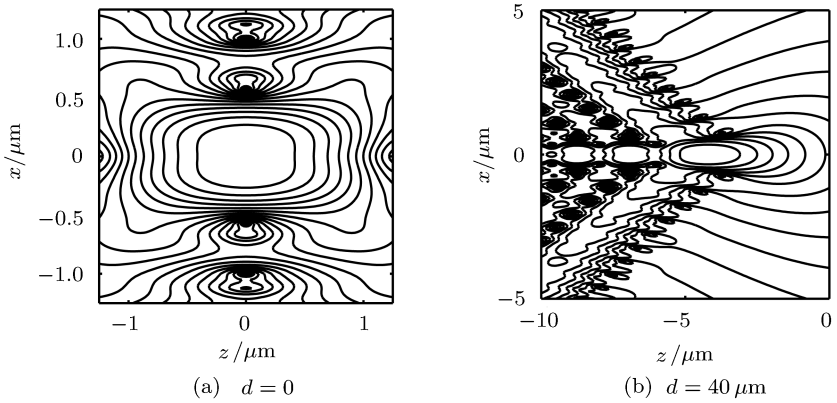


Fig.3. The contours of second-harmonic polarization distributions in xz plane.

Figures 2 and 3 give the contours of second-harmonic polarization distributions in the xy and xz plane (all pass the position of focus), respectively. Figure 2(a) and 3(a) correspond to the distributions for the probe depth $d = 0$ (free of aberration), whereas Fig.2(b) and Fig.3(b) represent the distributions for $d = 40$ μm. Those results show that refractive index mismatch has no effect on the symmetry of second-harmonic polarization distributions in the xy plane. However, the distributions in the xz plane becomes asymmetrical about the focal plane when $d = 40$ μm. At the same time, the peak intensity of second-harmonic polarization shifts along the negative z direction. Those characteristics are similar to those of the electric field distribution and primarily induced by spherical aberration introduced by refractive index mismatch,[10] due to the dependency of second-harmonic polarization on the excitation field.

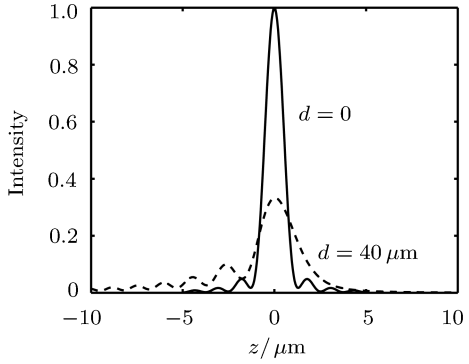


Fig.4. Second-harmonic polarization distributions at the z axis.

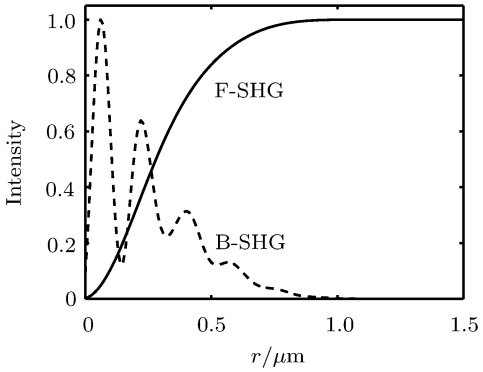


Fig.5. Changes in B-SHG and F-SHG with the sample radius for $d = 0$.

The generated second-harmonic signal can be detected in the forward or backward direction.[1] Because forward-(F-) SHG and backward-(B-) SHG change differently with sample thickness, for simplicity, a hypothetical collagen fibril in ideal 1-dimensional line is assumed to locate at the z axis and the axis of symmetry is parallel to the z axis. The second-harmonic polarization distributions along the z axis are plotted in Fig.4. The polarization intensities are normalized with respect to the maximum of second-harmonic polarization without aberration. For $d = 40$ μm, it should be noticed that the position of the peak intensity of second-harmonic polarization is set to be the coordinate origin. From Fig.4, it is obvious that refractive index mismatch can result in peak intensity degradation, increase secondary lobes and extension of polarization intensity profile. When $d = 0$, i.e. without refractive index mismatch, Fig.5 gives the changes in the detected B-SHG and F-SHG power with the radius (r) of the sample which centres at the focus. The intensities of B-SHG and F-SHG signal are normalized, respectively. According to Fig.5, the F-SHG intensity increases with r and becomes saturated when r is greater than about 1 μm, whereas the B-SHG intensity reaches its maximum at r values of about 0.075 μm and exhibits several secondary maxima. In addition, the B-SHG signal is negligible for large r. The difference between B-SHG and F-SHG can be explained by coherence effects and Gouy phase shift.[12,15,16]

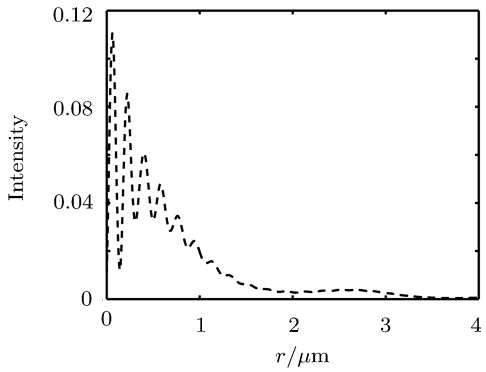


Fig.6. Change in B-SHG with sample radius for $d = 40$ μm.

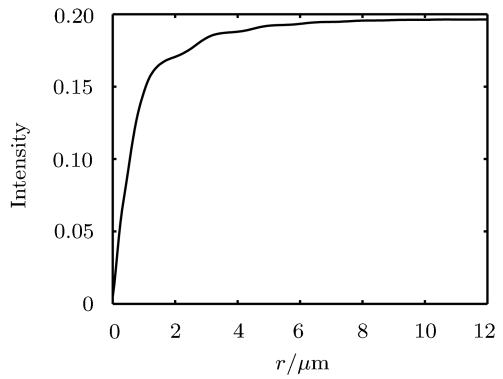


Fig.7. Change in F-SHG with sample radius for $d = 40$ μm.

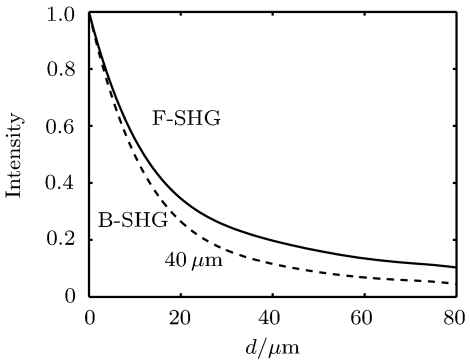


Fig.8. Changes in peak amplitude of B-SHG and F-SHG with increasing probe depth.

For $d = 40$ μm, the changes in B-SHG and F-SHG with r are given by Figs.6 and 7, respectively. B-SHG intensity also reaches its maximum when r is about 0.075 μm. But the peak intensity decays to be about 11% of the maximum of B-SHG intensity when $d = 0$, because of the attenuation of polarization intensity. From Fig.7, with the attenuation of polarization intensity, the F-SHG intensity also decreases. However, at $r = 1$ μm, it is not saturated but increases until r reaches about 10 μm, because the effective sample thickness responsible to F-SHG intensity, gets larger with extension of second-harmonic polarization distribution. The variations of maximum of B-SHG and F-SHG at different probe depths are plotted in Fig.8. It is obvious that both B-SHG and F-SHG decrease significantly as the observation depth moving to deeper regions, which can be an important factor to limit the imaging depth of SHG microscopy inside thick samples. In addition, F-SHG intensity decays more slowly than B-SHG, because of the combination of extension of second-harmonic polarization distribution and strong dependency of F-SHG signal on sample thickness.

4. Conclusion

SHG microscopy has been demonstrated to be a powerful tool for obtaining three-dimensional information in biology and materials science. There often occurs refractive index mismatch when the imaging plane is moved toward deeper regions inside the sample. Based on the vector diffraction theory, we have studied the effects of refractive index mismatch on the property of SHG microscopy by using Green's function approach to resolve the far-field radiation of SHG. The results indicate that refractive index mismatch can result in peak amplitude degradation, increase secondary lobes and extension of second-harmonic polarization distribution. At the same time, the polarization distribution in xz plane is not symmetrical about the focal plane again, because of aberration introduced by refractive index mismatch. B-SHG and F-SHG are numerically evaluated as functions of the sample radius and probe depth. Because of the attenuation of polarization intensity, both them significantly decrease with increasing probe depth, which can limit the imaging depth of SHG microscopy inside thick samples. A comparison between signal degradation in F-SHG and B-SHG shows that F-SHG intensity decays more slowly than B-SHG intensity, due to the combination of extension second-harmonic polarization distribution and strong dependence of F-SHG signal on sample thickness.

References

[1] Tai S P, Tsai T H, Lee W J, Shieh D B, Liao Y H, Huang H Y, Zhang K Y J, Liu H L and Sun C K 2005 *Opt. Express* **13** 8231
[2] Campagnola P J, Wei M D, Lewis A and Loew L M 1999 *Biophys. J.* **77** 3341
[3] Chu S W, Chen S Y, Chern G W, Tsai T H, Chen Y C, Lin B L and Sun C K 2004 *Biophys. J.* **86** 3914
[4] Sun C K, Chu S W, Chen S Y, Tsai T H, Liu T M, Lin C Y and Tsai H J 2004 *J. Struct. Biol.* **147** 19
[5] Yuan J H, Xiao F R, Wang G Y and Xu Z Z 2005 *Chin. Phys.* **14** 935
[6] Kleinman D A, Ashkin A and Boyd G D 1966 *Phys. Rev.* **145** 338
[7] Yew E Y S and Sheppard C J R 2006 *Opt. Express* **14** 1167
[8] Ma Y H, Zhao J L, Wang W L and Huang W D 2005 *Acta Phys. Sin.* **54** 2084 (in Chinese)
[9] Török P, Varga P, Laczik Z and Booker G R 1995 *J. Opt. Soc. Am.* A **12** 325
[10] Török P，Varga P and Booker G R 1995 *J. Opt. Soc. Am.* A **12** 2136
[11] Born M and Wolf E 2005 *Principle of Optics* (Beijing: Publishing House of Electronics Industry) (in Chinese)
[12] Boyd R W 1992 *Nonlinear Optics* (Boston: Academic)
[13] Chew W C 1992 *Waves and Fields in Inhomogeneous Media* (Beijing: Publishing House of Electronics Industry) (in Chinese)
[14] Novotny L 1997 *J. Opt. Soc. Am.* A **14** 105
[15] Cheng J X and Xie X S 2002 *J. Opt. Soc. Am.* B **19** 1604
[16] Volkmer A, Cheng J X and Xie X S 2001 *Phys. Rev. Lett.* **87** 023901-1